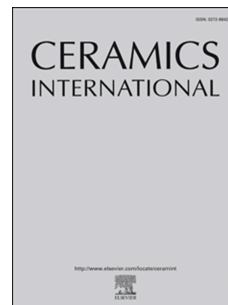


Journal Pre-proof



Structural and magnetic characterisation of BaTiO₃-BaFe₁₂O₁₉ bilayer thin films: interface effects on the magnetic properties of barium hexaferrite layer

C.I. Zandalazini, M.I. Oliva, J.C. Ferrero

PII: S0272-8842(21)00968-8

DOI: <https://doi.org/10.1016/j.ceramint.2021.03.275>

Reference: CERI 28340

To appear in: *Ceramics International*

Received Date: 21 October 2020

Revised Date: 22 March 2021

Accepted Date: 25 March 2021

Please cite this article as: C.I. Zandalazini, M.I. Oliva, J.C. Ferrero, Structural and magnetic characterisation of BaTiO₃-BaFe₁₂O₁₉ bilayer thin films: interface effects on the magnetic properties of barium hexaferrite layer, *Ceramics International*, <https://doi.org/10.1016/j.ceramint.2021.03.275>.

This is a PDF file of an article that has undergone enhancements after acceptance, such as the addition of a cover page and metadata, and formatting for readability, but it is not yet the definitive version of record. This version will undergo additional copyediting, typesetting and review before it is published in its final form, but we are providing this version to give early visibility of the article. Please note that, during the production process, errors may be discovered which could affect the content, and all legal disclaimers that apply to the journal pertain.

© 2021 Elsevier Ltd and Techna Group S.r.l. All rights reserved.

Structural and magnetic characterisation of BaTiO₃-BaFe₁₂O₁₉ bilayer thin films: interface effects on the magnetic properties of barium hexaferrite layer

C. I. Zandalazini¹

Consejo Nacional de Investigaciones Científicas y Técnicas, INFIQC, X5000IUS Córdoba, Argentina.

Universidad Nacional de Córdoba, Departamento de Fisicoquímica, Facultad de Ciencias Químicas, Centro Láser de Ciencias Moleculares, X5000IUS Córdoba, Argentina.

M. I. Oliva

Consejo Nacional de Investigaciones Científicas y Técnicas IFEG X5000HUA Córdoba, Argentina

Universidad Nacional de Córdoba, Facultad de Matemática, Astronomía, Física, y Computación, Grupo Ciencia de Materiales X5000HUA Córdoba, Argentina.

J. C. Ferrero

Consejo Nacional de Investigaciones Científicas y Técnicas, INFIQC, X5000IUS Córdoba, Argentina.

Universidad Nacional de Córdoba, Departamento de Fisicoquímica, Facultad de Ciencias Químicas, Centro Láser de Ciencias Moleculares, X5000IUS Córdoba, Argentina.

Abstract

We report the successful growth of BaFe₁₂O₁₉-BaTiO₃ (BaM-BTO) bilayer thin films using pulsed laser deposition, considering different crystallographic textures; BTO on (0001)-BaM and BaM on (100)-BTO. Our study involved the bilayers,

*Corresponding author

Email address: zc@famaf.unc.edu.ar (C. I. Zandalazini)

¹Present address: Consejo Nacional de Investigaciones Científicas y Técnicas, IFEG X5000HUA Córdoba, Argentina. Phone:+54 0351 4334051; ext. 41121.

the individual ferrite and titanate films, and the targets used in their growth. Raman spectroscopy and X-Ray diffraction were used to examine the structure of BaM-BTO thin films, indicating that there is no formation of impurity phases. The morphological characterization was made by scanning electron microscopy, and the magnetic behaviour was studied using SQUID magnetometry. The spontaneous magnetization, magnetic anisotropy constant, and anisotropy field were determined simultaneously from the magnetic hysteresis loop. In addition, we also studied the influence of different annealing temperatures over the magnetic behaviour of bare BaM and covered with BTO thin film. This allows to discern between the different magnetization reversal processes in bilayer systems, indicating a strong correlation between the anisotropy field and the coercive field, and an unusual linear relation of the anisotropy constant with the spontaneous magnetization. Our results indicate a direct influence of the BTO on the magnetic properties of the BaM phase, which places these composite bilayers as excellent candidates for the development of multifunctional devices.

Keywords: Ferrites, BaTiO₃, Magnetic properties, Functional applications

1. Introduction

Integrating different functions in one material system is currently a hot topic in science and engineering circles. This is the case of the so-called multifunctional materials (MF), materials that have the ability to perform multiple functions in a system due to their specific properties. Their huge potential for technological applications is presented in various areas, such as microwave devices, sensors, energy harvesting, photovoltaic technologies, among others [1–3]. However, much experimental effort has been invested investigating new composite MF, since MF

intrinsic (single-phase) materials are scarce [4, 5]. For example, the study of the materials referred to as multiferroics, which combines at least two ferroic orders (ferroelectric, ferromagnetic, or ferroelastic) [1, 4, 6] has taken great interest because in some of these MF materials, the magnetization can be controlled by an applied electric field, and vice versa, the electric polarization can be controlled by an applied magnetic field. This phenomenon, called magnetoelectric effect (ME) [7, 8], is several times greater in the composite MF than in intrinsic MF [9, 10]. It is in this sense that the MF bilayer compounds have recently gained great interest. The BaTiO₃ (BTO) is a ferroelectric perovskite ($T_C^{FE}=393$ K), photoreactive and with piezoelectric properties [11]; has a tetragonal structure at room temperature ($a = 0.398$ nm, $c = 0.401$ nm). The BTO was one of the main materials used in the generation and detection of acoustic energy devices, but it is now extensively studied its applications in nonlinear optics, supercapacitors, and microwave filters [12, 13], among others. The BaFe₁₂O₁₉ phase (BaM) is a ferrimagnetic (FerriM) material, with Néel temperature $T_N = 723$ K, presents magnetostrictive and piezomagnetic properties, and crystallizes in a complex hexagonal structure of space group $P6_3/mmc$ ($a = 0.588$ nm, $c = 2.32$ nm) [9, 10, 14, 15]. It contains two formula unit with a total of 64 ions, the 24 Fe³⁺ ions per unit cell occupy separately three kinds of octahedral sites (12k, 4f₂, and 2a), one tetrahedral site (4f₁), and one bipyramid site (2b). There are 16 Fe³⁺ ions in the 2a, 12k, and 2b sites that spin upward, whereas the remaining eight Fe³⁺ ions spinning downward are located in the 4f₁ and 4f₂ sites [14]. The arrangement of the ions of Fe³⁺ leads to a spontaneous magnetization of $20 \mu_B$ per unit cell and a high magnetocrystalline anisotropy with the c-axis as preferential direction. In addition to its well-known technological applications [9], it is currently one of the irreplaceable components

for the next-generation of magnetic microwave devices [10]. On the other hand, simultaneous occurrence of ferroelectricity, pyroelectricity, and ferromagnetism have been observed in bulk and thin films of barium hexaferrite [16–18], whereby it is presented as a promising candidate for future multiferroic-based memory devices.

Studies on BTO-BaM heterostructures have already been reported [10]. In particular, the BTO-BaM composites with core–shell heterostructure were successfully synthesized [19]. But a remarkable efforts have been done to develop laminated bilayer and multilayer multifunctional composites as thin films, due that in this configuration there are not conductive inclusions into the composite layer, which lead to remarkable magneto-electric coupling coefficients of a few $V/(cm.Oe)$ [2, 20].

In this work, we present a study of structural, morphological, and magnetic properties of BTO-BaM bilayer thin films. Maintaining the same growth conditions of films in bilayer configuration, we also prepared and characterized films of each individual phase. This allows to distinguish between intrinsic effects of each phase and those that are products of the interface between them. All samples were grown by pulsed laser deposition (PLD) technique. Vibrational spectra of both, targets and their respective thin films, were analysed by Raman spectrometry, and the structural and morphological analysis was performed by x-ray diffraction (XRD) and scanning electron microscopy (SEM), respectively. Magnetic measurements were performed using a superconducting quantum interference device (SQUID).

2. Experimental details

2.1. Samples preparation

Stoichiometric BTO and BaM ceramic targets were prepared pressing (600 MPa) high purity commercial powder of BTO and BaM, respectively. The pellets were sintered by an annealing in air to 1000°C during 300 minutes, thus obtaining target insulators and magnetically unpolarized (BaM) prior to the ablation process. The films were deposited by pulsed laser deposition technique, using a Nd-YAG laser in its second harmonic ($\lambda = 532$ nm) operated at a repetition rate of 10 Hz. The laser beam was focused on rotating target, using a plano-convex lens at an angle of 45°, resulting in an elliptical laser spot area of 0.012 cm². The incident laser fluence were adjusted in 1.0 J/cm² and 1.8 J/cm² (per pulse) for growth of the BTO and the BaM phase, respectively. The deposition time for the BTO was 30 minutes, while for the BaM it was 15 minutes, thus obtaining approximately 140 nm and 70 nm of film thicknesses in BTO and BaM, respectively. The deposition chamber was initially evacuated with the aid of a diffusion pump to pressures in the 10⁻⁷ Torr range, subsequently was introduced high purity oxygen to reach a stable pressure at 2.5 mTorr and 150 mTorr for BTO and BaM phases growth, respectively. The distance between the target and the substrate was maintained at 3.5 cm, and the substrate deposition temperature was fixed at 650°C for all samples prepared. Two configurations were considered for the preparation of the bilayers, BaM/BTO on (100)LaAlO₃, and BTO/BaM on (0001)Al₂O₃, called respectively samples FT and TF. The substrate crystallographic orientation was chosen to achieve preferential growth in each corresponding phase. After the deposit has been completed, it was immediately cooled down, to room temperature, into a constant pressure of 50 Torr of O₂. Our previous study of the effects of laser parameters, and the proposed

experimental arrangement, allowed us to avoid the effect of classical heating of the material when UV-lasers are not used for the growth of oxides [21].

TABLE I

Besides, maintaining the same growth conditions listed above, we also prepared BTO on (100)LaAlO₃ (sample T), and BaM on (0001)Al₂O₃ (sample F) single phase as reference samples. In which was considered the in-situ annealing that each one receives when they form the corresponding bilayer system, i.e., after completing the growth of the BTO (BaM) film, both the substrate temperature and growth pressure used in the growth of the BaM (BTO) film in the FT (TF) bilayer are maintained for 15 min. (30 min). All samples (FT, TF, T, F), received an ex-situ annealing treatment, maintaining them at 900°C for 20 minutes in air atmosphere. Furthermore, in order to obtain a better description of the magnetic behaviour of the c-axis-textured BaM system, the samples with BaM on Al₂O₃ were also studied before ex-situ annealing (indicated as samples F₀ and TF₀). Nomenclature used for all the samples are listed in Table I.

2.2. Instrumentations

For structural characterizations, XRD patterns were recorded in a Philips PW 3830 diffractometer using Cu-K_α line in $\theta/2\theta$ configurations, and Raman spectra were measured at room temperature, using a LabRAM HR from HORIBA Jobin Yvon excited with Ar⁺ laser ($\lambda = 514.5$ nm) in the backscattering configuration, equipped with an air cooled CCD detector. Scanning electron microscopy images were performed with a SEM Carl Zeiss SIGMA, and magnetization measurements were performed at different temperatures (5-300 K) with a SQUID from Quantum

Design.

3. Results and discussion

3.1. Raman characterization

Raman spectroscopic technique is one of the useful methods to gain insight into the microscopic structural effects of materials. Crystal defects, distortion of the lattice, or an excursion of the components could be shown in Raman bands. Raman vibrational spectra of targets and bilayer thin films are shown in figure 1. The spectra were deconvolved, after background subtraction, using the Gaussian distributions. The characteristic frequencies of each sample, obtained by means of the above-mentioned adjustment, are listed in Table II, where also including the appropriate symmetry assignments.

In the ferroelectric phase BTO (tetragonal BTO), there are 5 atoms in the unit cell, and give rise to 12 optical modes. Due to the long-range electrostatic forces, optical modes splits into the transverse (TO) and longitudinal (LO) components [22–24]. The Raman spectrum of BTO target show typical features agree well with previous reports. A dip near 180 cm^{-1} , which has been previously observed in the Raman spectra of BTO, and is the result of interference between Raman scattering from two vibrational modes with overlapping frequency ranges, resulting in a "negative peak" [23, 25]. Next are a broad peak centring near 261 cm^{-1} , a narrow peak at 306 cm^{-1} , an asymmetric broad peak near 518 cm^{-1} , and a broad weak peak at about 720 cm^{-1} [22, 23]. The Raman peaks at 306 cm^{-1} and 720 cm^{-1} are specific to the tetragonal phase of BTO.

On the other hand, in the BaM structure, the 64 atoms per unit cell on 11 different symmetry sites, give rise to 189 wavelength optical modes ($3 \times 64 - 3$), 42 Ra-

man active modes ($11A_{1g}+14E_{1g}+17E_{2g}$), 30 infrared active modes ($13A_{2u}+17E_{1u}$), and 54 infrared and Raman inactive modes [14, 26]. In our samples, all frequencies observed of the Raman peaks of the target BaM present a good correspondence with the assignments of the mode frequencies in polycrystalline BaM samples[14, 26, 27]. The peaks at 171 and 183 cm^{-1} to E_{1g} vibration of whole spinel blocks [14], while the peaks at 615 cm^{-1} , 686 cm^{-1} and 716 cm^{-1} are attributed to A_{1g} vibration at the $4f_2$, 2b and $4f_1$ sites, respectively. The peak at 413 cm^{-1} is due to A_{1g} vibration at the mixed vibrations involving mainly 12k and 2a sites. Other peaks at 289, 315, 338, 378, 466 cm^{-1} are attributed to the vibration of Fe–O bonds of all the octahedral at the 12k, 2a, and $4f_2$ sites [14, 28].

TABLE II

It is worth to note that, in both bilayer thin films, the BTO and BaM phases had no significant changes in relation to these phases in bulk ($\pm 2 \text{ cm}^{-1}$), and are in accordance with Raman spectra of target used. According to Raman spectra analysis reported by Y. Lu *et al.* [29], the measurement of phonons with E_{1g} symmetry in BaM-phase is indicative of a polycrystalline sample, which means that both bilayer thin films contains polycrystalline grains of BaM-phase (or at least disoriented crystals of this phase). In the FT bilayer, the phonon mode observed at 489 cm^{-1} is attributed to the LAO substrates [30], and in the case of TF bilayer, Raman spectrum shows a phonon mode at 343 cm^{-1} , associated to Al_2O_3 substrate [31].

3.2. Structural and morphological characterization

3.2.1. Single-phase thin films

The diffraction patterns corresponding to the BTO thin film (T) and its respective BTO-target (TBTO) are shown in the top of figure 2. Both samples present a tetrahedral structure of BTO, and according to PCPDF:83-1880 chart [32], BTO thin film on (100)-LaAlO₃ shows a preferential (100) orientation (partly promoted by the LAO substrate, as in previous reports [30, 33]). An average crystallite size of 29 nm was roughly estimated by the usual Scherrer's formula [34]. In the bottom of figure 2 are shown the diffraction patterns of sample F and its respective BaM-target (TBaM). In both samples, a hexagonal crystallographic structure of the BaM is observed, and in total agreement with the PCPDF:84-0757 chart [32]. From this last reference, it is possible to determine that thin film growth occurs preferentially in the planes (0001)-BaM on (0001)-Al₂O₃. The average crystallite size of 23 nm was estimated. It should be noted that no peaks of impurity phases were observed. Although the diffraction due to the K_{β} -Cu and K_{α} -W emissions were filtered (typically representing less than 0.5% of the total), the high count rates recorded in the oriented planes of the substrates (about 6×10^5 cps), make this is notorious in relation to the peaks associated with the film. This is a typical feature of the use of $\theta/2\theta$ geometry in thin films [30, 35].

The SEM images of samples T and F are presented in figure 3. Single-phase BTO shows a predominant morphology of island or Volmer-Weber growth mode [36]. This type of growth occurs when the force of attraction between atoms is stronger than that which hold them with the substrate, subsequently, with the increase in film thickness, these structures coalesce to form larger grains. According to results from XRD analysis presented above, the preferential growth induced by

substrate is observed too in these island. In the case of the single-phase BaM, there are two modes of growth; one through hexagonal plate-like shapes (50 to 500 nm), and another one with grains with random orientation. Whereas XRD analysis suggest as predominant the first above mentioned growth mode, it is hoped that this layer is the majority regarding the second mode of growth, which indicates that the first stage is governed by a growth layer by layer, i.e., hexagonal grain will grow by a 2D nucleation, commonly called Frank-van der Merwe growth [37, 38]. Although the high energy of the species that arrive to the substrate encourages growth of these concentric islands, the main cause of obtained preferential orientation is due to the chosen substrate. The (0001) Al_2O_3 promote that the first deposited layers of BaM copy their structure, whereupon, this influence can be reduced as thickness increase and starting to be energetically more favourable orienting themselves with c-axis in plane. It should be mentioned that ferrites grow most rapidly in their a-b plane to form hexagonal platelets [39, 40], and if in its initial nucleation process, the platelets have their c-axis perpendicular to the substrate plane, they can grow fast laterally without restriction (the basal plane is parallel to the substrate surface). Contrary to this, if in the initial growth process such order is not presented, the crystal growth will be prohibited by adjacent grains with different c-axis directions due to space restriction [29].

3.2.2. Bilayers thin films

Figures 4 show diffraction patterns of the bilayer FT (top) and TF (bottom). In the bilayer FT, BTO phase remain unchanged and presents the same preferential growth as sample T, while BaM phase, grown in this case on BTO, has a polycrystalline structure, thus indicating the relevance of the substrate for obtaining a crystallographic orientation. These results are in total agreement with the XRD

analysis of single phase films presented above.

With respect to the diffractogram of the sample TF, a preferential growth in the c-axis for the BaM phase on Al_2O_3 and a polycrystalline growth for BTO phase on BaM film is observed. However, from the Raman analysis presented previously, it can be inferred that the crystallographic order is not total in the BaM phase, since vibration modes associated with polycrystalline ferrite were observed in this sample (peak at 183 cm^{-1} , phonons with E_{1g} symmetry). This means that there is a significant amount of BaM microcrystallites in-plane c-axis orientation besides c-axis orientation normal to the plane of substrate. This is mainly due to the high sensitivity of the Raman spectroscopy (about 5 lattice parameter of coherence length) against XRD (about 20 lattice parameter of coherence length), which allows to detect microcrystallites [27]. In both samples are not observed others additional phases peaks, which implies that there is no formation of impurity phases in the interface or product of diffusion of elements. The structural parameters of each sample are listed in Table III (the peaks were fitted using the pseudo-Voigt function approximation method [41]).

TABLE III

Figures 5 show SEM images of samples FT (left) and TF (right). BaM phase on BTO film present a compact surface structure of elongated acicular-like, with lengths ranging from 100 to 300 nm and an average diameter of 40 nm. In the case of BTO phase on BaM film, a not completely compact coverage is observed, which could be associated to effects related to the surface of the BaM film, which presented typical characteristics of disordered hexagonal plate-like shapes (see Fig. 3, second stage of growth).

3.3. Magnetic properties

Magnetic properties studies were carried out by measuring hysteresis loops at different temperatures and by recording Zero Field Cooling - Field Cooling curves (ZFC-FC). The hysteresis loops for temperatures between 10 and 300 K are presented at the top and at the bottom of the figure 6, sample FT and sample TF, respectively. The magnetic field was applied in the direction parallel to the surface of the film ($H_{//}$), and the diamagnetic (and eventually also paramagnetic phase) contribution of the substrate was subtracted to consider only the ferrimagnetic contribution. The hysteresis loops of TBaM (not shown) exhibit typical ferrimagnetic behaviour of barium hexaferrite in bulk ($M_S = 340 \text{ emu/cm}^3$, $Sq = 0.54$, $H_C = 3890 \text{ Oe}$) [39], while TBTO and T (in bulk, non-magnetic material), presented only their diamagnetic contribution, indicating the absence of a soft ferromagnetic behaviour associated with oxygen deficiency, which has been observed in BTO nanoparticles [42, 43].

In order to estimate the magnetocrystalline anisotropy constant K_1 and magnetic anisotropy field H_A , we used the law of approach by saturation method [44], which describe the relation between magnetization (M) and magnetic field (H_{app}). For crystals with hexagonal symmetry, this law can be expressed as:

$$M(T, H) = M_S(T) \left[1 - \frac{H_A^2}{15H^2} \right] + H \cdot \chi(T) \quad (1)$$

where M_S and H_A are fitting parameters, and represent the spontaneous magnetization and anisotropy field, respectively. The anisotropy field H_A gives a measure of the strength of the anisotropy effect and torque necessary to take the magnetization away from the easy axis, and for uniaxial crystals, $H_A = \frac{2K_1}{M_S}$. The other fitting parameter is the χ , that represent the high-field differential suscepti-

bility, which is usually very small and could be neglected. We fit the $M(H, T)$ curves using equation 1 in the region of high magnetic fields (M_S , H_A , and χ as fitting parameters). The spontaneous magnetization (M_S), coercive fields (H_C), and squareness ratio ($S_q = M_R/M_S$) are shown in the Table IV.

TABLE IV

Regarding the sample FT, the M_S at 300 K is 294 emu/cm³ (382 emu/cm³ in BaM "bulk" [45]), in total agreement with reported values for polycrystalline BaM thin films [46, 47]. Reducing the temperature to 10 K, M_S is increased by 57% from its value at room temperature (RT), comparable with the recently reported by M. Shalini *et al.* [47]. The authors presented results of temperature-dependent magnetic properties of nanocrystalline barium hexaferrite indicating an increase of about 40% over the RT magnetization. Thus, the growth of BaM on BTO film shows a typical magnetic behaviour of a pure polycrystalline BaM film, with no appreciable interface effects with BTO film.

On the other hand, sample TF (c-axis oriented BaM phase) shows a strong decrease in the M_S , representing approximately a 68% of its corresponding value in sample FT, and such reduction is observed equally for all temperatures considered. The fact that the M_S is smaller for the TF as compared to the FT sample was tentatively attributed to strain effects on the magnetic properties of BaM, which is manifested as a result of its structural configuration. That is, after the growth process, and during the cooling process in the TF sample, the BaM-phase is subjected to strain induced by both the Al₂O₃-substrate and the BTO-layer, which has influence on the magnetic properties of the entire BaM film (more details can be

found in [48]). In addition, the impact of ex-situ annealing on structural relaxation in the BaM-phase of the TF sample is less than the FT sample. This conjecture is also partially supported by our study of the annealing effect in BaM/Al₂O₃ bare (see Table V and the corresponding discussion, samples F₀ and F), where after ex-situ annealing, BaM reaches a magnetization of 316 emu/cm³, similar to that obtained in the BaM on BTO (294 emu/cm³, sample FT). It should be mentioned that although there could be an influence of the diffusion of elements (Fe/Ti, see detailed analysis below), the presence of secondary phases was not observed.

This drastic reduction is also observed in the other magnitudes considered, H_C and S_q , representing in sample TF 35-40% of their corresponding values in sample FT. With respect to the S_q ($= M_R/M_S$) values, the preferential growth in the c-axis for the BaM phase in TF sample indicate that the easy axis of magnetization is perpendicular to the sample plane. Thus, the magnetization left behind in TF after the external magnetic field (in-plane applied field) has been removed will be less than the corresponding one in the FT sample (in-plane easy axis of magnetization). On the other hand, although H_C is affected by many factors (domain structure, shape and magnetic anisotropy effects, inter-granular interactions, among others) [39, 49], in BaM with grain size less than 1 μm , the H_C will increase with a decrease in grain size. That is, in the single-domain regime, the major factor determining the H_C in BaM is attributed to the pinning of magnetization at the grain boundaries (that act as pinning centers), which leads to an increase in H_C in small grain samples (for more details see [50]). Our results suggest that the configuration chosen for the growth of the TF sample favors the grains growth with respect to the FT sample (see also the discussion in section 3.2.1). This dependence on grain size has also been observed in the F₀ y F samples, where ex-situ

annealing causes about 40% reduction of H_C initial value (see Table V). However, in both samples a similar trend of magnetic behaviour with temperature is observed, while M_S and H_C show a reduction with increasing temperature, the S_q values remain approximately independent of it, typical in uniaxial anisotropy ferrites [39, 49, 51]. As a consequence of the reduction in thermal energy, the strengthening in the superexchange interaction leads to an increase in the magnetization. As can be seen in Table IV, the temperature dependence of the M_S for FT and TF are nearly linear as a result of the ferrimagnetic ordering (in the particular case of BaM, this is mainly attributed to the temperature dependence of the Fe^{3+} (12k, octahedral site) sublattice magnetization) [39, 52]. The increased coercivity with decreasing temperature would indicate that in our BaM thin films, the single-domain weakly-interacting nanograins are predominant. The reduction of the effects of thermal fluctuations would lead to the freezing of the larger magnetic moments into anisotropic directions, therefore, to an increase in the effective anisotropy, which is directly proportional to the coercivity in the thin films. The observed behavior of coercivity is consistent with the results of previous studies on BaM thin film fabricated by PLD [18] (and references therein), and in M-type doped BaM nanocrystalline powders [53].

Figures 7 show the magnetization of samples FT and TF, measured as a function of temperature in ZFC and FC states (an in-plane applied field of 0.025 T). Both samples show similar magnetic behaviour, Neel temperature above of 300 K ($T_N=723$ K in BaM bulk [45]), and the irreversibility temperatures measured (temperature to which are separated curves ZFC-FC) were 285 K and 265 K for FT and TF, respectively. A particular feature is observed at temperatures below

30 K, where in both samples, the abrupt increase in magnetization could indicate the existence of a minority paramagnetic phase, which is activated at low temperatures. This characteristic of the $M(T)$ has been associated with the presence of frustrated spins in the nano-sized grain boundary region, giving rise to a behavior known as surface paramagnetism [54, 55]. We analyze the low temperature upturn using Curie type equation, $\chi_{SP}(T) = M/H = C/T^\gamma$, where $\chi_{SP}(T)$ is the surface magnetic susceptibility, C is the surface Curie constant, and γ is the exponent to estimate the surface magnetism in the temperature dependence of magnetization curves. Based on MFC(T) data, the fit parameters (C, γ) for the FT and TF samples were $(8.7E-8, 0.025)$ and $(1.2E-7, 0.018)$ respectively. Considering that C is proportional to the number of surface paramagnetic spins ($C = N \cdot \mu_{SP}/3k_B$, where μ_{SP} is the effective surface paramagnetic moment of each spin, and k_B is the Boltzmann constant [54]), and that an increase in γ indicates a greater paramagnetic contribution ($\gamma = 1$, ideal paramagnet), it is expected that systems with smaller grain size present lower values of C . This is totally consistent with previous reports ([18, 54]), and with our analysis on the coercive fields in both samples; smaller grain size (FT sample), greater interactions among the interfacial spins between grains. We return to this discussion in our analysis of the ex-situ annealing effects. In the inset of figure 7 (right) shows the fit data of TF and FT samples using temperature dependence of magnetization curves.

This may be related to an interdiffusion layer formed in the ex-situ annealing process, whereby composition or structure effects could be present. In the first case, during the annealing process could be an interdiffusion of Ti/Fe on the BaM/BTO films, thus enabling the interlayer formation of Ti-doped BaM [56] or Fe-Doped BTO [57], but this could be dismissed as there is no observable sec-

ondary phase via our Raman and XRD analysis. The second case, where the structural effects could be change magnetic behaviour, will be discussed below.

In the inset of figure 7 (left) are shown the K_1 versus M_S for different temperatures. The linear relation between K_1 and M_S is clearly seen in both samples. This unusual linear dependence of the anisotropy constant with the saturation magnetization has also been recently reported by J. Wang *et al.* [58]. The authors studied silica-coated $\text{BaFe}_{12}\text{O}_{19}$ platelets, and also found that temperature dependence of the K_1 is not framed in the established by the theoretical predictions for hexagonal crystals, which requires a new theory to explain. Regarding the inversion of magnetic moments processes in a system, commonly, if this involve mostly rotation processes, K_1 estimated by initial susceptibility (ψ_{in} , being $K = (1/2)M_S^2/\psi_{in}$, and $\psi_{in} = M/H$) should give similar values that obtained from equation 1. But the K_1 values obtained using initial susceptibility represent approximately 50% of those corresponding to those obtained by Eq. 1, which allows to infer the presence of mechanism other than coherent rotation. However, although the magnetization dependence of the magnetic anisotropy is similar in both samples, in TF it decays more rapidly (and reaching lower K values) as compared to the FT. This characteristic could be associated with intrinsic parameters involving the reduction of the magnetic anisotropy, as previously mentioned, in sample TF, the strains are initiated at the interfaces of the BaM-layer sandwiched between the Al_2O_3 -substrate and BTO-layer, and have an influence on the magnetic properties of the entire BaM film. It is well known that the in BaM, the major contribution to the magnetic anisotropy comes from Fe^{3+} at octahedral (4f2 and 12k) and bi-pyramid (2b) sites [40, 59], and hence the grain size growth in sample TF induces tilting in the angle of Fe-O-Fe bonds, which could be related to spin-canting behavior

Ex-situ annealing and magnetic properties of crystallographically oriented barium hexaferrite.

In order to analyse the effects of ex-situ annealing on the magnetic properties of systems, we also study the systems as-prepared, in particular, in the systems with crystallographically oriented BaM (samples F_0 , F, TF_0 , and TF) Table V show the coercive fields (H_C) and squareness ratio ($S_q = M_R/M_S$) for different temperatures. It can be inferred that during the BTO layer growth, there are no significant changes in the coercive field of the as-prepared samples (F_0 and TF_0). However, the annealing treatment has different effects on the final magnetic properties of the systems. It is observed that in the case of bare ferrite, ex-situ annealing causes about 40% reduction of H_C initial value. As previously indicated, this could be associated with an increase in grain size (annealing treatment effect), which leads to a reduction of the efforts in the inversion of magnetic moments. While in the case of the ferrite covered with BTO, the H_C values are increased by 60% compared to the as prepared system, which could be attributed mainly to annealing effects on the grain-boundary magnetic structure (effective anisotropy of the system), rather than to changes in grain size. In other words, the increase in strains due to the annealing effect on the BaM layer (layer sandwiched between substrate and BTO-layer) would lead to an increase in the spin disorder around grain boundaries, which influence the surface anisotropy. Since the superexchange mechanism depends strongly on the angle made by Fe-O-Fe bonds, any structural disorder near the grain boundary (stress, oxygen non-stoichiometry, vacancies, among others) modifies this exchange and leads to a spin disorder, with direct consequences on

the pinning of magnetization at the grain boundaries (thus increasing the H_C).

TABLE V

In figure 8(a) are shown ZFC-FC curves of four samples, where it is observed that only bilayer samples exhibit the disordered surface spins behaviour for temperatures below 30 K, which was previously discussed and associated with a surface paramagnetism behaviour, due to the presence of the nano sized grains. To better understand the processes involved at low temperatures we have fitted the $M_S(T)$ data with the Bloch's Law (Eq. 2 [60]), where the exponent $\alpha = 3/2$ for FerriM and FM bulk materials. To the right of the figure 8(c) are shown the $M_S(T)$ for different samples before and after annealing treatment. Our data showed an excellent fitting of the bare and bilayer BaM data, according to the parameters corresponding typical value to BaM bulk ($\alpha=1.5$) [58]. The latter could be indicating that surface spin effects in the interface region (such as spin canting, spin freezing, spin disorder), observed at low temperature, is not reflected in the Bloch's law parameters. In addition, assuming a mean-field approach, the presence of a second magnetic phase from the irreversible susceptibility ($\psi_{irr} = dM/dH$) is not observed (not shown here).

$$M_S(T) = M_S(0) \left[1 - \left(\frac{T}{T_0} \right)^\alpha \right] \quad (2)$$

Figure 8(b) shows a strong correlation between H_A and H_C in the four systems. In the case of bare BaM, the ex-situ annealing does not essentially modify the dependence between these quantities, and present similar correlation that reported to BaM thin films [49, 51, 61]. However, in bilayer samples, the coating

process with BTO leads to a considerable increase in the H_A values of BaM layer, without significantly affecting the H_C values (curves F_0 and TF_0), which are affected by ex-situ annealing and reduces the correlation between both quantities (in TF sample, H_A remains almost constant up to 150 K). This loss of correlation may be associated with spin canting, as previously discussed.

4. Conclusions

Successfully were deposited bilayers of $BaFe_{12}O_{19}$ and $BaTiO_3$ considering both polycrystalline and textured growth by frequency-doubled Nd:YAG laser. Our study involved not only the bilayers, but also the individual films and the targets used in their growth, which allowed to distinguish between intrinsic properties of the phases and those corresponding to the interface. From Raman and XRD analysis in the bilayer thin films, no secondary crystallographic phases were observed. Magnetic measurements indicate a strong dependence of magnetic and structural properties with the substrate used to growth the BaM phase, and from ZFC-FC curves of the bilayers, after of ex-situ annealing, the presence of spin canting effects at low temperature was evidenced. Bilayer thin films show no evidence of secondary magnetic phases by ψ_{irr} analysis, but a loss of correlation between the anisotropy field and the coercive field was observed. In addition, an unusual linear relation of the anisotropy constant with the spontaneous magnetization, dependency that is currently under investigation. Although is necessary a more detailed discussion about a possible diffusion of Ti (Fe) into BaM (BTO) thin film, our results might indicate a direct influence of the BTO on the magnetic properties of the BaM phase, which places these composite bilayers as excellent candidates for the development of multifunctional devices.

Acknowledgements

The authors acknowledge financial support from the Consejo Nacional de Investigaciones Científicas y Técnicas (CONICET), the Universidad Nacional de Córdoba (SECYT-UNC), and PME 2006–1544.

References

- [1] N. A. Spaldin, R. Ramesh, Advances in magnetoelectric multiferroics, *Nature Mater.* 18 (2019) 203–212. doi:10.1038/s41563-018-0275-2.
- [2] P. Galizia, M. Algueró, N. Bernier, N. Gambacorti, E. Aza, A. Lappas, M. Venet, C. Galassi, Magnetoelectric dual-particulate composites with wasp-waisted magnetic response for broadband energy harvesting, *J. Alloys and Compd.* 783 (2019) 237–245. doi:10.1016/j.jallcom.2018.12.273.
- [3] A. Lendlein, R. S. Trask, Multifunctional materials: concepts, function-structure relationships, knowledge-based design, translational materials research, *Multifunct. Mater.* 1 (2018) 010201. doi:10.1088/2399-7532/aada7b.
- [4] H. Schmid, Multi-ferroic magnetoelectrics, *Ferroelectrics* 162 (1994) 317–338. doi:10.1080/00150199408245120.
- [5] P. Nguyen, B. Sarpi, F. Petronio, C. Mocuta, P. Ohresser, D. Stanescu, J. Moussy, A. Vlad, A. Resta, E. Otero, B. Belkhou, J. Leroy, N. Jedrecy, H. Magnan, A. Barbier, $Mn_{0.7}Fe_{2.3}O_4$ Nanoplatelets Embedded in $BaTiO_3$

- Perovskite Thin Films for Multifunctional Composite Barriers, *ACS Appl. Nano Mater.* 3 (2020) 327–341. doi:10.1021/acsanm.9b01970.
- [6] R. Ramesh, N. Spaldin, Multiferroics: progress and prospects in thin films., *Nature Mater* 6 (2007) 21–29. doi:10.1038/nmat1805.
- [7] L. D. Landau, E. M. Lifshitz (Eds.), *Electrodynamics of Continuous Media*, Pergamon, Oxford, 1960.
- [8] M. Venet, W. Santa-Rosa, P. S. da Silva Jr., J. C. M'Peko, P. Ramos, H. Amorín, M. Algueró, Selection and Optimization of a $K_{0.5}Na_{0.5}NbO_3$ -Based Material for Environmentally-Friendly Magnetoelectric Composites, *Materials* 13 (2020) 731. doi:10.3390/ma13030731.
- [9] R. C. Pullar, Hexagonal ferrites: A review of the synthesis, properties and applications of hexaferrite ceramics, *Prog. Mater. Sci.* 57 (2012) 1191–1334. doi:10.1016/j.pmatsci.2012.04.001.
- [10] A. Srinivas, R. Gopalan, V. Chandrasekharan, Room temperature multiferroism and magnetoelectric coupling in $BaTiO_3$ - $BaFe_{12}O_{19}$ system, *Solid State Commun.* 149 (2009) 367–370. doi:10.1016/j.ssc.2008.12.013.
- [11] J. M. Moulson, A. J. Herbet (Eds.), *Electroceramics: Materials, Properties, Applications*, Second Ed., John Wiley & Sons, Ltd. New Jersey, 2003.
- [12] E. K. Nyutu, C.-H. Chen, P. K. Dutta, S. L. Suib, Effect of microwave frequency on hydrothermal synthesis of nanocrystalline tetragonal barium titanate, *J. Phys. Chem. C* 112 (2008) 9659–9667. doi:10.1021/jp7112818.

- [13] M. Sharma, A. Gaur, J. K. Quamara, Swift heavy ions irradiated *PVDF/BaTiO₃* film as a separator for supercapacitors, *Solid State Ionics* 352 (2020) 115342. doi:10.1016/j.ssi.2020.115342.
- [14] W. Y. Zhao, P. Wei, X. Y. Wu, W. Wang, Q. J. Zhang, Lattice vibration characterization and magnetic properties of M-type barium hexaferrite with excessive iron, *J. Appl. Phys.* 103 (2008) 063902. doi:10.1063/1.2884533.
- [15] C. Yu, A. S. Sokolov, P. Kulik, V. G. Harris, Stoichiometry, phase, and texture evolution in PLD-Grown hexagonal barium ferrite films as a function of laser process parameters, *J. Alloys and Compd.* 814 (2020) 152301. doi:10.1016/j.jallcom.2019.152301.
- [16] G. Tan, X. Chen, Structure and multiferroic properties of barium hexaferrite ceramics, *J. Magn. Magn. Mater.* 327 (2013) 87–90. doi:10.1016/j.jmmm.2012.09.047.
- [17] P. Kumar, A. Gaur, Signature of multiferroicity and pyroelectricity close to room temperature in *BaFe₁₂O₁₉* hexaferrite, *Ceram. Int.* 43 (2017) 16403–16407. doi:10.1016/j.ceramint.2017.09.016.
- [18] P. Kumar, A. Gaur, Room temperature multiferroicity for *BaFe₁₂O₁₉* thin film fabricated by pulsed laser deposition technique, *Appl. Phys. A* 125 (2019) 629. doi:10.1007/s00339-019-2928-7.
- [19] G. Schileo, C. Pascual-Gonzalez, M. Alguero, I. M. Reaney, P. Postolache, L. Mitoseriu, K. Reichmann, M. Venet, A. Feteira, Multiferroic and magnetoelectric properties of *Pb_{0.99}[Zr_{0.45}Ti_{0.47}(Ni_{1/3}Sb_{2/3})_{0.08}]O₃-CoFe₂O₄* mul-

- tilayer composites fabricated by tape casting, *J. Europ. Ceramic Soc.* 38 (2018) 1473–1478. doi:10.1016/j.jeurceramsoc.2017.10.055.
- [20] H. Palneedi, V. Annapureddy, S. Priya, J. Ryu, Status and perspectives of multiferroic magnetoelectric composite materials and applications, *Actuators* 5 (2016) 9. doi:10.3390/act5010009.
- [21] C. I. Zandalazini, M. I. Oliva, J. C. Ferrero, Highly c-axis oriented ZnO thin films on glass substrate by pulsed laser deposition: fluence-dependent effects., *J. Nanoelectron. Optoelectron.* 14 (2019) 1461–1467. doi:10.1166/jno.2019.2576.
- [22] U. D. Venkateswaran, V. M. Naik, R. Naik, High-pressure Raman studies of polycrystalline $BaTiO_3$, *Phys. Rev. B* 58 (1998) 14256–14260. doi:10.1103/PhysRevB.58.14256.
- [23] V. P. Pavlovic, M. V. Nikolic, V. B. Pavlovic, J. Blanusa, S. Stevanovic, V. V. Mitic, M. Scepanovic, B. Vlahovic, Raman Responses in Mechanically Activated $BaTiO_3$, *J. Am. Ceram. Soc.* 97 (2014) 601–608. doi:10.1111/jace.12423.
- [24] M. Alguero, J. M. Gregg, L. Mitoseriu (Eds.), *Nanoscale Ferroelectrics and Multiferroics: Key Processing and Characterization Issues, and Nanoscale Effects*, John Wiley and Sons, Inc., USA, 2016.
- [25] L. H. Robins, D. L. Kaiser, L. D. Rotter, P. K. Schenck, G. T. Stauff, D. Rytz., Investigation of the structure of barium titanate thin films by Raman spectroscopy, *J. Appl. Phys.* 76 (1994) 7487. doi:10.1063/1.357978.

- [26] J. Kreisel, G. Lucazeau, H. Vincent, Raman spectra and vibrational analysis of $BaFe_{12}O_{19}$ hexagonal ferrite, *J. Solid State Chem.* 137 (1998) 127–137. doi:10.1006/jssc.1997.7737.
- [27] J. Kreisel, S. Pignard, H. Vincent, J. Sénateur, G. Lucazeau, Raman study of $BaFe_{12}O_{19}$ thin films, *Appl. Phys. Lett.* 73 (1998) 1194–1196. doi:10.1063/1.122124.
- [28] C. Wu, Z. Yu, Y. Yang, K. Sun, J. Nie, Y. Liu, X. Jiang, Z. Lan, Computational and experimental study on the cat on distribution of La-Cu substituted barium hexaferrites, *J. Alloys and Compd.* 664 (2016) 406–410. doi:10.1016/j.jallcom.2015.12.251.
- [29] Y. F. Lu, W. D. Song, Properties of $BaFe_{12}O_{19}$ films prepared by laser deposition with in situ heating and post annealing, *Appl. Phys. Lett.* 76 (2000) 490–492. doi:doi.org/10.1063/1.125797.
- [30] K.-M. Yeung, C.-L. Mak, K.-H. Wong, G. K.-H. Pang, Preparation of $BaTiO_3$ thin films of micrometer range thickness by Pulsed Laser Deposition on (001) $LaAlO_3$ substrates, *J. J. Appl. Phys.* 43 (2004) 6292–6296. doi:10.1143/JJAP.43.6292.
- [31] J. Lewis, D. Schwarzenbach, , H. D. Flack, Electric field gradients and charge density in corundum $\alpha - Al_2O_3$, *Acta Crystall.* A38 (1982) 733–739. doi: <http://rruff.info/tags=152/X080006>.
- [32] JCPDS-International Centre for Diffraction DataPCPDFWIN data: 84-0757(BaM) and 83-1880(BTO) charts, Powder Diffraction FileTM (PDF) (1998).

- [33] Y. Lee, J. D. Achenbach, M. J. Nystrom, S. R. Gilbert, B. A. Block, B. W. Wessels, Line-focus acoustic microscopy measurements of Nb_2O_5/MgO and $BaTiO_3/LaAlO_3$ thin-film/substrate configurations, IEEE Trans. Ultrason., Ferroelect., Freq. Cont. 42 (1995) 376–380. doi:10.1109/58.384445.
- [34] A. Patterson, The scherrer formula for x-ray particle size determination, Phys. Rev. 56 (1939) 978–982. doi:10.1103/PhysRev.56.978
- [35] M. Tyunina, J. Narkilahti, J. Levoska, D. Chvostova, A. Dejneka, V. Trepakov, V. Zelezny, Ultrathin $SrTiO_3$ films epitaxy and optical properties, J. Phys.: Condensed Matter 21 (2009) 232203. doi:10.1088/0953-8984/21/23/232203.
- [36] Y. Wang, W. Chen, B. Wang, Y. Zheng, Ultrathin ferroelectric films: Growth, characterization, physics and applications, Materials 7 (2014) 6377–6485. doi:10.3390/ma7096377.
- [37] X. Y. Zhang, C. K. Ong, S. Y. Xu, H. C. Fang, Observation of growth morphology in pulsed-laser deposited barium ferrite thin films, Appl. Surf. Sci. 143 (1999) 323–327. doi:10.1016/S0169-4332(99)00100-2.
- [38] P. Shepherd, K. K. Mallick, R. J. Green, Magnetic and structural properties of M-type barium hexaferrite prepared by co-precipitation, J. Magn. Magn. Mater. 311 (2007) 683–692. doi:10.1016/j.jmmm.2006.08.046.
- [39] R. C. O’Handley (Ed.), Modern Magnetic Materials, J. Wiley and Sons, New York, USA, 2000.
- [40] R. B. Jotania, S. H. Mahmood (Eds.), Magnetic Oxides and Composites:

- Tuning the Magnetic Properties of M-type Hexaferrites (Ch. 2), Vol. 31, Materials Research Foundations, 2018. doi:10.21741/9781945291692-2.
- [41] V. Soleimanian, S. R. Aghdaee., Comparison methods of variance and line profile analysis for the evaluation of microstructures of materials, Powder Diffraction 23 (2008) 41–51. doi:10.1154/1.2888763.
- [42] Y. Slimani, M. A. Almessiere, S. E. Shirsath, E. Hannachi, G. Yasin, A. Baykal, B. Ozçelik, I. Ercan, Investigation of structural, morphological, optical, magnetic and dielectric properties of $(1-x)\text{BaTiO}_3/x\text{Sr}_{0.92}\text{Ca}_{0.04}\text{Mg}_{0.04}\text{Fe}_{12}\text{O}_{19}$ composites, J. Magn. Magn. Mater. 510 (2020) 166933. doi:10.1016/j.jmmm.2020.166933.
- [43] A. Sundaresan, R. Bhargavi, N. Rangarajan, U. Siddesh, C. N. R. Rao, Ferromagnetism as a universal feature of nanoparticles of the otherwise nonmagnetic oxides, Phys. Rev. B 74 (2006) 161306. doi:10.1103/PhysRevB.74.161306.
- [44] S. Chikazumi (Ed.), Physics of Magnetism, Wiley, New York, USA, 1964.
- [45] G. Bertotti (Ed.), Hysteresis in Magnetism, Academic Press, USA, 1998.
- [46] D. A. Vinnik, A. Y. Tarasova, D. A. Zherebtsov, S. A. Gudkova, D. M. Galimov, V. E. Zhivulin, E. A. Trofimov, S. Nemrava, N. S. Perov, L. I. Isaenko, R. Niewa, Magnetic and structural properties of barium hexaferrite $\text{BaFe}_{12}\text{O}_{19}$ from various growth techniques, Materials 10 (2017) 578. doi:10.3390/ma10060578.
- [47] M. G. Shalini, A. Subha, B. Sahu, S. C. Sahoo, Phase evolution and temperature dependent magnetic properties of nanocrystalline barium hexafer-

- rite, *J. Mat. Sci: Materials in Electronics* 30 (2019) 13647–13654. doi: 10.1007/s10854-019-01734-x.
- [48] S. R. Shinde, R. Ramesh, S. E. Lofland, S. M. Bhagat, S. B. Ogale, R. P. Sharma, T. Venkatesan, Effect of lattice mismatch strains on the structural and magnetic properties of barium ferrite films, *Appl. Phys. Lett.* 72 (1998) 3443. doi:10.1063/1.121660.
- [49] M. A. Almessiere, Y. Slimani, A. Baykal, Structural and magnetic properties of Ce-doped strontium hexaferrite, *Ceram. Int.* 44 (2018) 9000–9008. doi: 10.1016/j.ceramint.2018.02.101.
- [50] J. Dho, E. K. Lee, J. Y. Park, N. H. Hur, Effects of the grain boundary on the coercivity of barium ferrite $\text{BaFe}_{12}\text{O}_{19}$, *J. Magn. Mater.* 285 (2005) 164–168. doi:10.1016/j.jmmm.2004.07.033.
- [51] M. A. Almessiere, Y. Slimani, H. S. E. Sayed, A. Baykal, S. Ali, I. Ercan, Investigation of microstructural and magnetic properties of $\text{BaV}_x\text{Fe}_{12-x}\text{O}_{19}$ nanohexaferrites, *J. Supercond. Nov. Magn.* 32 (2018) 1437–1445. doi: 10.1007/s10948-018-4856-8.
- [52] A. Isalgué, Exchange Interactions in $\text{BaFe}_{12}\text{O}_{19}$, *Appl. Phys. A* 39 (1986) 221–225. doi:10.1007/BF00620738.
- [53] X. Battle, M. G. del Muro, J. Tejada, H. Pfeiffer, P. Gornert, E. Sinn, Magnetic study of m-type doped barium ferrite nanocrystalline powders, *J. Appl. Phys.* 74 (1993) 3333. doi:10.1063/1.354558.
- [54] N. Naresh, R. N. Bhowmik, B. Ghosh, S. Banerjee, Study of surface

- magnetism, exchange bias effect, and enhanced ferromagnetism in alpha- $\text{Fe}_{1.4}\text{Ti}_{0.6}\text{O}_3$ alloy, *J. Appl. Phys.* 109 (2011) 093913. doi:10.1063/1.3585663.
- [55] R. N. Bhowmik, R. Nagarajan, R. Ranganathan, Magnetic enhancement in antiferromagnetic nanoparticle of CoRh_2O_4 , *Phys. Rev. B* 69 (2004) 054430. doi:10.1103/PhysRevB.69.054430.
- [56] X. Batlle, X. Obradors, J. Rodríguez-Carvajal, M. Pernet, M. V. Cabañas, M. Vallet, Cation distribution and intrinsic magnetic properties of Co-Ti-doped M-type barium ferrite, *J. Appl. Phys.* 70 (1991) 1614. doi:10.1063/1.349526.
- [57] H. T. Langhammer, T. Müller, T. Walther, R. Böttcher, D. Hesse, E. Pip-pel, S. G. Ebbinghaus, Ferromagnetic properties of barium titanate ceramics doped with cobalt, iron, and nickel, *J. Mater. Sci.* 51 (2016) 10429. doi:10.1007/s10853-016-0263-3.
- [58] J. Wang, F. Zhao, W. Wu, G.-M. Zhao, Unusual temperature dependence of the magnetic anisotropy constant in barium ferrite, *J. Appl. Phys.* 110 (2011) 096107. doi:10.1063/1.3657851.
- [59] Q. Pankhurst, Anisotropy field measurement in barium ferrite powders by applied field mossbauer spectroscopy, *J. Phys.: Cond. Matter* 3 (1991) 1323. doi:10.1088/0953-8984/3/10/010.
- [60] F. Bloch, Zur theorie des ferromagnetismus, *Z. Physik* 61 (1930) 206—219. doi:10.1007/BF01339661.

- [61] T. L. Hylton, M. A. Parker, J. K. Howard, Preparation and magnetic properties of epitaxial barium ferrite thin films on sapphire with in-plane, uniaxial anisotropy, *Appl. Phys. Lett.* 61 (1992) 867–869. doi:10.1063/1.107772.

Journal Pre-proof

Figure 1: (Top) Raman spectra, and their corresponding deconvolution spectra, of targets used (samples TBaM and TBTO). (Bottom) Raman spectra of bilayer thin films (samples FT and TF).

Journal Pre-proof

Figure 2: X-ray spectra of the BTO thin film (a), and target (b). X-ray spectra of the BaM thin film (c) and target (d). The peaks corresponding to the substrates are indicated by symbols (circles). All spectra are free of impurity phase peaks.

Figure 3: SEM images of BTO on (100)LaAlO₃ (sample T), and BaM on (0001)Al₂O₃ (sample F). In the latter, it is clear that hexagonal platelet structure in the initial growth process of BaM phase.

Figure 4: (Top) X-ray spectrum of the sample FT, the BTO phase present the same plane of the found in sample T, and the BaM phase, polycrystalline growth is indicate by presence of the peaks corresponding to (114) plane, and the others ones indicated in the figure. (Bottom) X-ray spectrum of the sample TF; a preferential growth for BaM phase, and polycrystalline growth in BTO phase can be observed.

Figure 5: SEM images of BaM on BTO (sample FT) and BTO on BaM (sample TF) bilayer thin films.

Figure 6: Hysteresis loops from SQUID measurements at different temperatures of samples FT (top) and TF (bottom).

Figure 7: ZFC-FC curves of samples FT (circle) and TF (box). The arrows toward the right indicate the ZFC curves and toward the left, FC curves. Inset: (Left) Magnetic anisotropy as a function of spontaneous magnetization determined by Eq. 1 (squares FT and circles is TF samples), and (right) Temperature dependence of magnetization data have been fitted to Curie type equation for at 250 Oe ($T < 30$ K, see text for more details).

Figure 8: (a) ZFC-FC curves for samples before and after ex-situ annealing, (b) H_A versus H_C (the arrow indicates temperature rise), and (c) M_S versus $T^{1.5}$ including their corresponding fitted curves by Eq. 2.

Table I: Nomenclature used for the samples studied. Crystallographic orientation of the substrates are (0001) and (100) for Al_2O_3 and LaAlO_3 , respectively. WA means sample without ex-situ thermal annealing (See details in the text).







Name	Sample description	Scheme
TBTO	BaTiO_3 target	
TBaM	$\text{BaFe}_{12}\text{O}_{19}$ target	
T	BaTiO_3 on LaAlO_3	
F	$\text{BaFe}_{12}\text{O}_{19}$ on Al_2O_3	
F ₀	$\text{BaFe}_{12}\text{O}_{19}$ on Al_2O_3 (WA)	
FT	$\text{BaFe}_{12}\text{O}_{19}/\text{BaTiO}_3$ on LaAlO_3	
TF	$\text{BaTiO}_3/\text{BaFe}_{12}\text{O}_{19}$ on Al_2O_3	
TF ₀	$\text{BaTiO}_3/\text{BaFe}_{12}\text{O}_{19}$ on Al_2O_3 (WA)	

Table II: Frequencies (cm^{-1}) of the active modes of bilayer thin films and their corresponding targets. We also include the vibrational modes of BTO and BaM in bulk, reported by U. Venkateswaran *et al.* [22] and J. Kreisel *et al.* [26], respectively.

Bilayers		Barium titanate			Barium hexaferrite		
FT	TF	TBTO	BTO[22]	Symmetry	TBaM	BaM[26]	Symmetry
		175	170	E(TO)	171		
184	183		180-185	E(TO),E(LO)-A ₁ (LO)	183	184	E _{1g}
249	249				249	250	E _{1g}
261	261	261	270	A ₁ (TO)			
308	306	306	305	E(TO+LO)	289	285	E _{1g}
338	338				315	317-319	(E _{1g} ,A _{1g})-E _{2g}
	343				338	335-340	E _{2g} -(A _{1g} ,E _{1g})
413	413				378	385	E _{2g}
489					413	409-417	A _{1g} -E _{1g}
518	520	518	518-520	E(TO)-A ₁ (TO)	466	467	A _{1g}
530	526				528	527-529	E _{1g} -E _{2g}
626	621				563	566	E _{2g}
691	689				615	614	A _{1g}
719	722	717	715-720	E(LO)-A ₁ (LO)	686	684	A _{1g}
					716	713	A _{1g}

Table III: Structural parameters of the targets and samples studied. The lattice parameters, and average crystallite size, are expressed in nm.

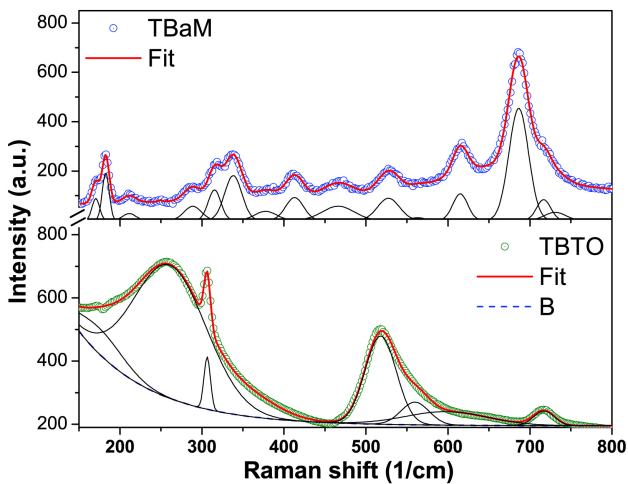
Sample	Barium titanate				Barium hexaferrite			
	a=b	c	c/a	D_{XRD}	a	c	c/a	D_{XRD}
TBTO	0.401	0.405	1.011	41				
TBaM					0.590	2.325	3.941	39
T	0.400	0.405	1.013	29				
F					-	2.310	-	23
FT	0.400	0.409	1.024	15				
					0.587	2.341	3.986	11
TF	0.397	0.406	1.022	17				
					-	2.312	-	15

Table IV: Coercive fields (H_C), spontaneous magnetization M_S , and squareness ratio ($S_q = M_R/M_S$) for different temperatures in the samples FT and TF.

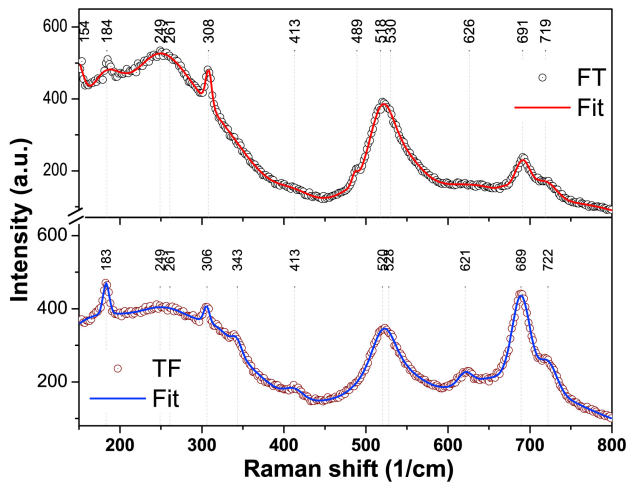
T (K)	H_C (Oe)		M_S emu/cm ³		S_q	
	FT	TF	FT	TF	FT	TF
10	3502	1344	462	329	0.61	0.26
50	3386	1183	455	325	0.61	0.24
150	3347	1111	412	285	0.60	0.23
200	3326	1122	381	253	0.59	0.23
250	3319	1114	348	227	0.58	0.23
300	3570	1084	294	190	0.61	0.21

Table V: Coercive fields (H_C) and squareness ratio ($S_q = M_R/M_S$) for different temperatures: (0001)-BaM single layer (samples F₀ and F), and BTO-(0001)-BaM bilayer (samples TF₀).

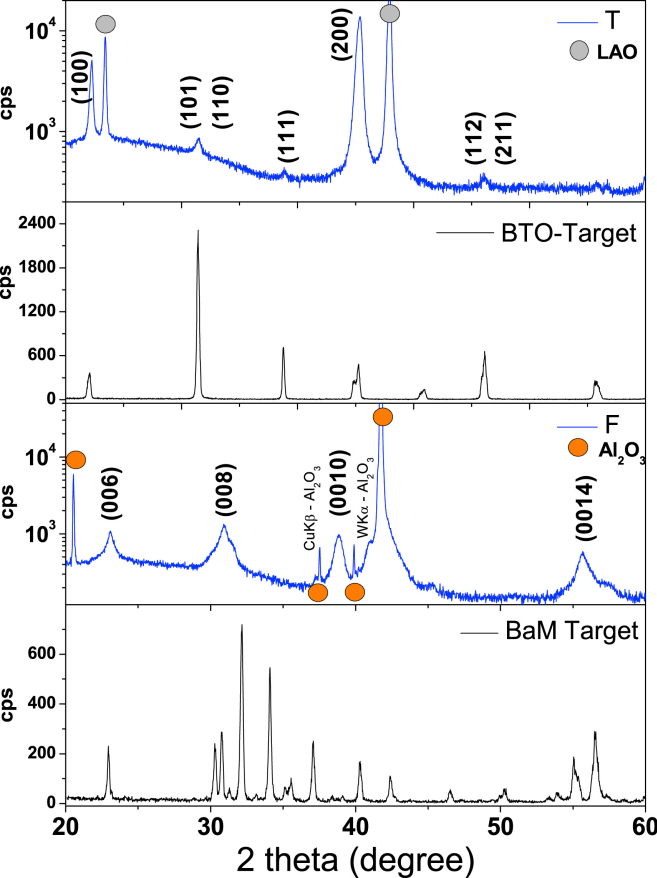
T (K)	H_C (Oe)				S_q			
	F ₀	F	TF ₀	TF	F ₀	F	TF ₀	TF
10	810	353	827	1344	0.43	0.30	0.32	0.26
50	650	340	671	1183	0.39	0.29	0.30	0.24
150	554	315	581	1111	0.33	0.28	0.27	0.23
200	516	300	549	1122	0.32	0.27	0.25	0.23
250	485	275	529	1114	0.31	0.27	0.26	0.23
300	394	261	577	1084	0.28	0.27	0.29	0.21

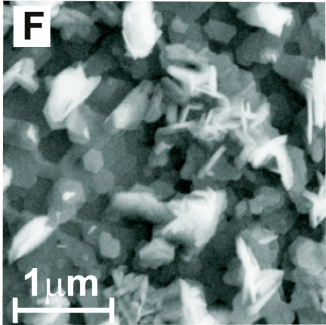
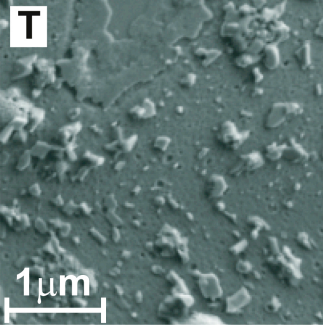


(a)

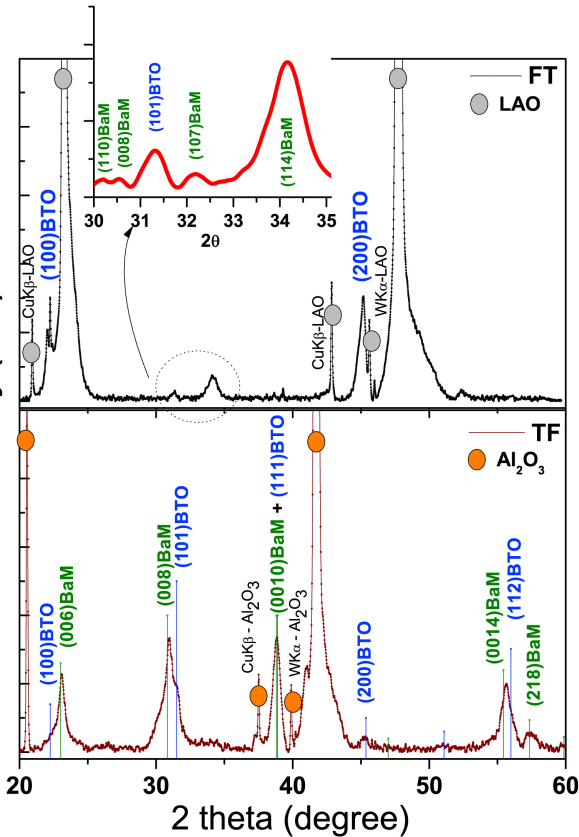


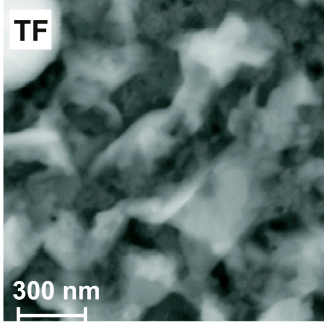
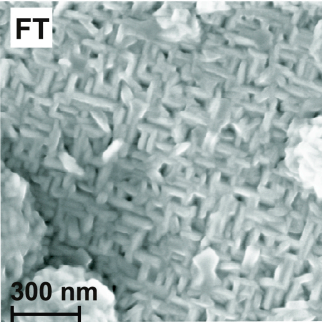
(b)

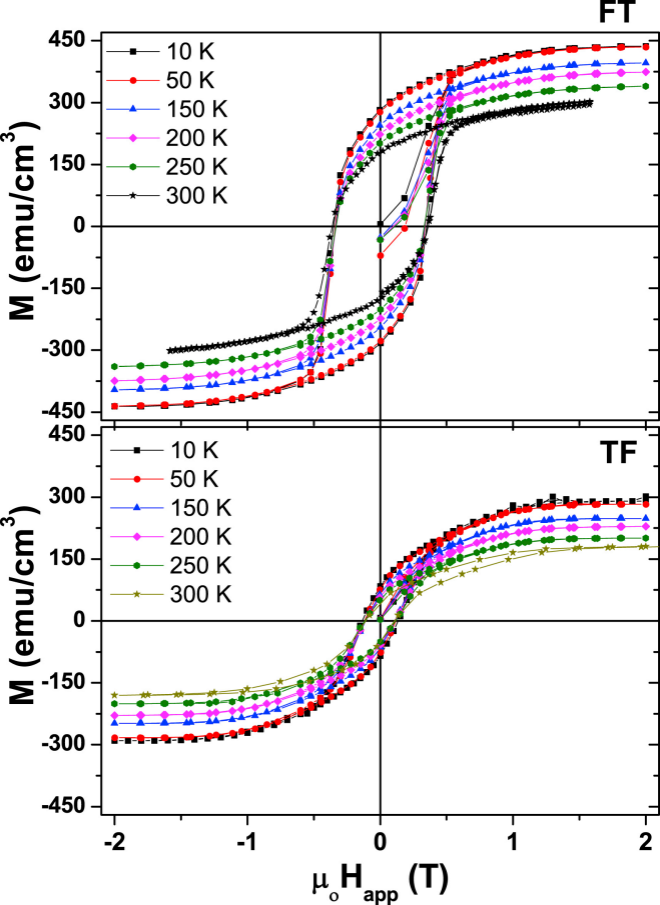


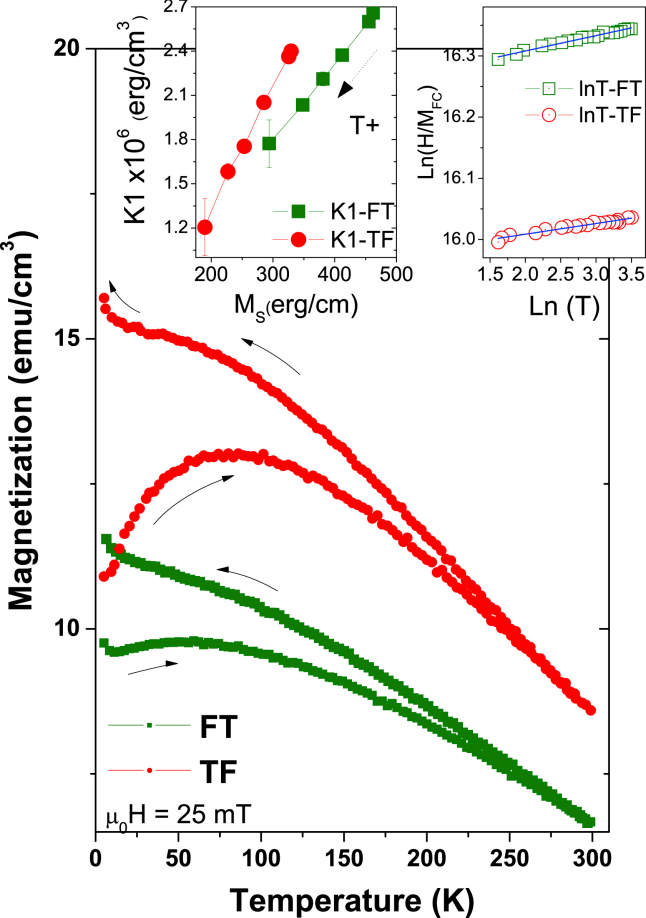


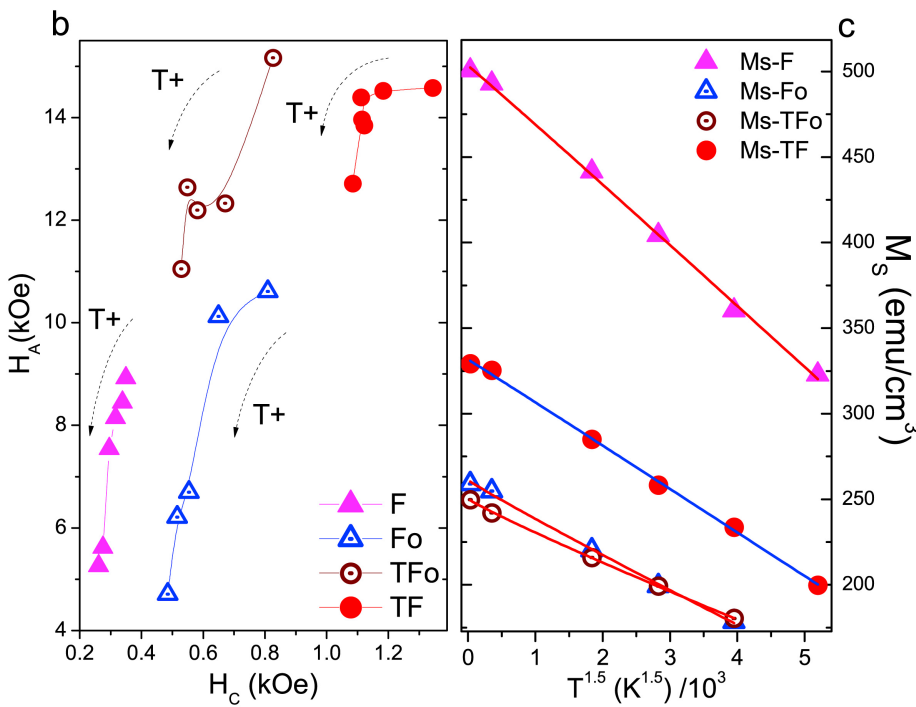
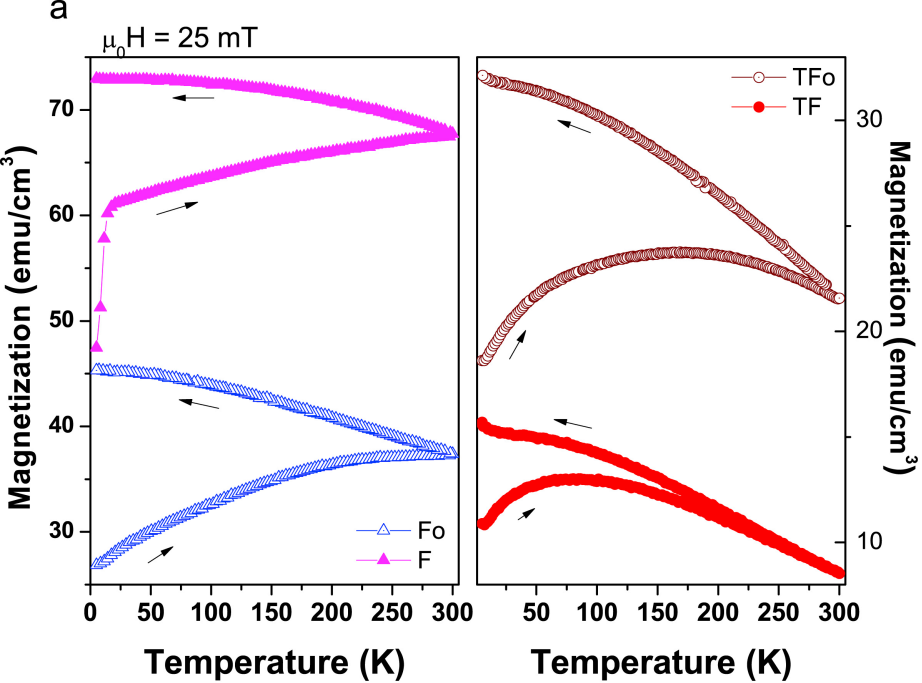
Intensity (a.u.)











Declaration of interests

The authors declare that they have no known competing financial interests or personal relationships that could have appeared to influence the work reported in this paper.

The authors declare the following financial interests/personal relationships which may be considered as potential competing interests:

Journal Pre-proof